

Stress analysis of the TMSR graphite component under irradiation conditions

Xiong Yang^{1,2} · Yan-Tao Gao¹ · Yang Zhong^{1,2} · Dong Ding^{1,2} · Derek-Kwong-Lai Tsang¹

Received: 5 January 2018 / Revised: 8 June 2018 / Accepted: 16 June 2018 / Published online: 15 November 2018
© Shanghai Institute of Applied Physics, Chinese Academy of Sciences, Chinese Nuclear Society, Science Press China and Springer Nature Singapore Pte Ltd. 2018

Abstract TMSR uses nuclear graphite as a neutron moderator, a reflector, and the structural material, and utilizes molten salt as a coolant. When running normally, the graphite components are immersed in the molten salt. Thus, the nuclear graphite comes into direct contact with the molten salt, which infiltrates the open pores of the nuclear graphite. This infiltration may influence the stress analysis of the graphite component. In this study, a User Material subroutine was used to analyze the stress distribution of the graphite component, both with and without molten salt infiltration. Many influence factors were taken into consideration, such as the dose gradient, the shape of the permeation zone, and the permeation area. The results show that the dose gradient, shape, and area of the permeation zone all significantly influence the stress distribution. Furthermore, the results of the stress analysis indicate that for a regular graphite component with a square cross section, the peak maximum principal stress value occurs at the center of the cross section, and the symmetry

of the maximum principal stress distributions was modified by quarter circle and half ellipse permeation zones.

Keywords Nuclear graphite · Stress analysis · Irradiation · Permeation zone

1 Introduction

The concept of a molten salt reactor (MSR) was established in the 1950s at Oak Ridge National Laboratory (ORNL, Tennessee, USA), in which the primary nuclear reactor coolant, or even the fuel itself, was a molten salt mixture. In 1954, the Aircraft Reactor Experiment (ARE), which reached a maximum power of 2.5 MWt, was designed for operation at a temperature of 1500 °F (1100 K), using a circulating fluoride salt fuel in a heterogeneous core [1]. ARE became critical and operated in a stable and self-regulating manner for 9 days, without mechanical or chemical problems. The continuation of this work led to the commissioning of the Molten-Salt Reactor Experiment (MSRE). The MSRE [2], an 8 MWt graphite-moderated reactor at ORNL, reached its criticality in 1965, was powered by molten fluoride salt at 1200 °F, which circulated through the core of graphite bars. Though the MSRE program ended in 1969; its result demonstrated the practicality and performance of molten salt power reactors. The success of this reactor and the expertise gained during this experiment led, in the 1970s, to the initiation of a new power reactor project, the Molten Salt Breeder Reactor (MSBR) [3].

Nowadays, there is a renewed interest in MSRs, which are believed to be a promising Generation IV reactor type [4]. There are several MSR development programs

This work was supported by the ‘‘Hundred Talent Program’’ of the Chinese Academy of Sciences, the Ministry of Human Resources and Social Security (No. Y419016031), and the Strategic Priority Research Program of Chinese Academy of Science (No. XDA02040100).

✉ Yan-Tao Gao
gaoyantao@sinap.ac.cn

✉ Derek-Kwong-Lai Tsang
zengguangli@sinap.ac.cn

¹ Shanghai Institute of Applied Physics, Chinese Academy of Sciences, Shanghai 201800, China

² University of Chinese Academy of Science, Beijing 100049, China

worldwide. For example, Terrestrial Energy Inc. (TEI), a Canada-based company, is developing a small modular reactor called the Integral Molten Salt Reactor (IMSR) [5], while Seaborg Technologies, a Danish company, is developing a core that utilizes a single high-temperature salt, and named it the Molten Salt Wasteburner (MSW) [6]. In 2011, a preliminary reactor system concept, for a Small modular Advanced High Temperature Reactor (SmAHTR) was described by researchers at ORNL, along with an integrated high-temperature thermal energy storage, or “salt vault” system [7]. The SmAHTR is a 125-MWt, liquid salt-cooled, coated particle-graphite-fueled, integral primary low-pressure system, operating at 700 °C. In the same year, China began the Thorium Molten Salt Reactor program (TMSR) [8, 9], which was based on the MSRE. Originally, a 2 MWt demonstration plant was built, which could then be scaled to commercial size. Within the next year, Japan, in order to prevent nuclear proliferation and terrorism and to minimize nuclear waste, presented a new nuclear program named FUJI [10].

The primary advantage of MSRs is the continuous adjustment of the fuel-salt composition, which ensures its operation over time, with no reactivity reserve. Moreover, it is possible to reach very high temperatures and power densities without large internal pressures, and therefore, the structural elements are unconstrained. However, in an MSR, the molten salt comes into direct contact with the graphite moderator and reflector, which may lead to changes to the graphite properties, such as the coefficient of thermal expansion and irradiation resistance, and may damage the graphite structure in particular circumstances [11]. The material test by ORNL [12] showed that salt permeation into the MSRE-specified graphite type was confined mostly to surface pits or to penetration along cracks, usually microscopic, that intersected the surfaces. Cracks and open pores intersect the surface of the graphite component increasing the total contact area between the molten salt and the graphite, which could cause the irradiation dose to increase inside the graphite. The material test also showed that almost any distribution of salt within the graphite will cause the local temperature to rise, even in regions of maximum heat flux. In this study, the cracks in the permeation zone were assumed to be longitudinal and propagating the full length of the graphite bar.

In addition, the graphite material properties are changed by rapid neutron irradiation as a function of the irradiation temperature and dose in the reactor. The fast neutron dose and the irradiation temperature decrease with distance from the center of the core to the boundary of the vessel; the graphite components are, therefore, subject to significant irradiation and temperature gradients. The irradiation dose and temperature variations across the large cross sections

of graphite components, in normal operation, generate internal stresses that could ultimately lead to component failure. In order to analyze the internal stress of the TMSR graphite component during irradiation and infiltration of molten salt, a User Material (UMAT) subroutine, containing irradiation-dependent constitutive relationships for graphite dimensional changes and the material properties of graphite, for example, the elastic modulus, the coefficient of thermal expansion, and irradiation creep, was developed by Tsang based on previous work [13–15]. This subroutine can be used together with the ABAQUS finite element program to perform time-integrated nonlinear irradiated graphite stress analyses, and the UMAT can be used for high temperatures up to ~ 1000 °C.

The effects of molten salt on stress distribution were analyzed under different conditions in this study.

2 The UMAT constitutive equations

In this section, the irradiated graphite constitutive equations are briefly presented. The new TMSR UMAT is designed for anisotropic materials. The total strain within irradiated graphite $\boldsymbol{\varepsilon}_{\text{total}}$ is the sum of five different strain components:

$$\boldsymbol{\varepsilon}_{\text{total}} = \boldsymbol{\varepsilon}_e + \boldsymbol{\varepsilon}_{\text{pc}} + \boldsymbol{\varepsilon}_{\text{sc}} + \boldsymbol{\varepsilon}_{\text{dc}} + \boldsymbol{\varepsilon}_{\text{th}}, \quad (1)$$

where $\boldsymbol{\varepsilon}_e$ is the elastic strain, $\boldsymbol{\varepsilon}_{\text{pc}}$ is the primary creep strain, $\boldsymbol{\varepsilon}_{\text{sc}}$ is the secondary creep strain, $\boldsymbol{\varepsilon}_{\text{dc}}$ is the dimensional change strain, and $\boldsymbol{\varepsilon}_{\text{th}}$ is the thermal strain, with or without stress.

2.1 Elastic strain

The elastic strain, $\boldsymbol{\varepsilon}_e$, is related to the stress, $\boldsymbol{\sigma}$, by Hooke’s law of linear elasticity, i.e.

$$\boldsymbol{\sigma} = \mathbf{D}\boldsymbol{\varepsilon}_e, \quad (2)$$

where \mathbf{D} is the material matrix. The material matrix is assumed to be a function of E_e , the Young’s modulus, and ν_e , Poisson ratio.

2.2 Creep strains

The primary creep strain, $\boldsymbol{\varepsilon}_{\text{pc}}$, is defined as

$$\frac{d\boldsymbol{\varepsilon}_{\text{pc}}}{d\gamma} = k_1 (\alpha \mathbf{D}_{\text{pc}} \boldsymbol{\sigma} - \boldsymbol{\varepsilon}_{\text{pc}}), \quad (3)$$

where γ is the radiation fluence, k_1 is the primary creep dose constant, α is the magnitude of asymptotic primary creep strain in elastic strain units, and \mathbf{D}_{pc} is the primary creep material matrix, which is a function of the primary

Fig. 1 (Color online) Different permeation zones in the graphite component. **a** Quarter circle, **b** half ellipse, **c** frame zone

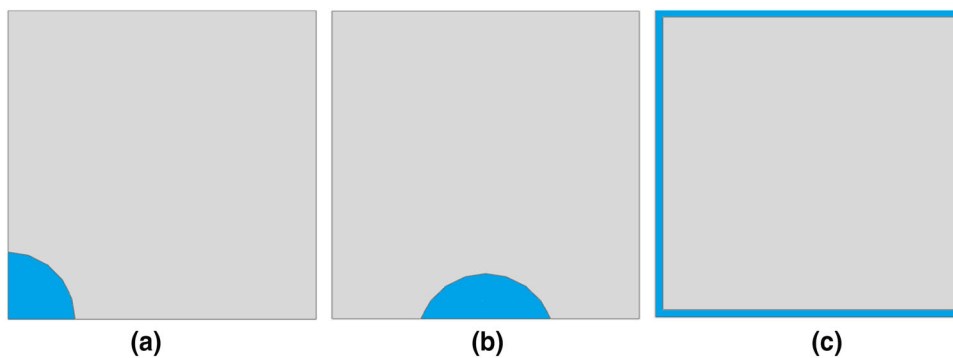


Fig. 2 (Color online) 2D finite element mesh. **a** Section with a quarter circle shaped permeation zone (PAR:0.005), **b** Section with an elliptical permeation zone (PAR:0.005), **c** Section with a frame permeation zone (PAR:0.005)

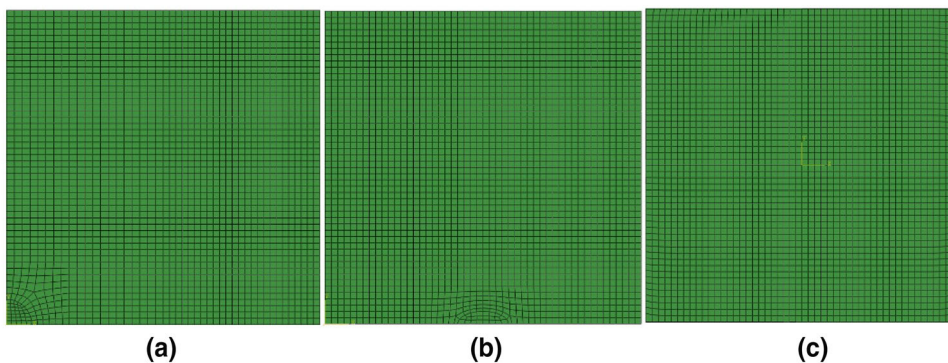
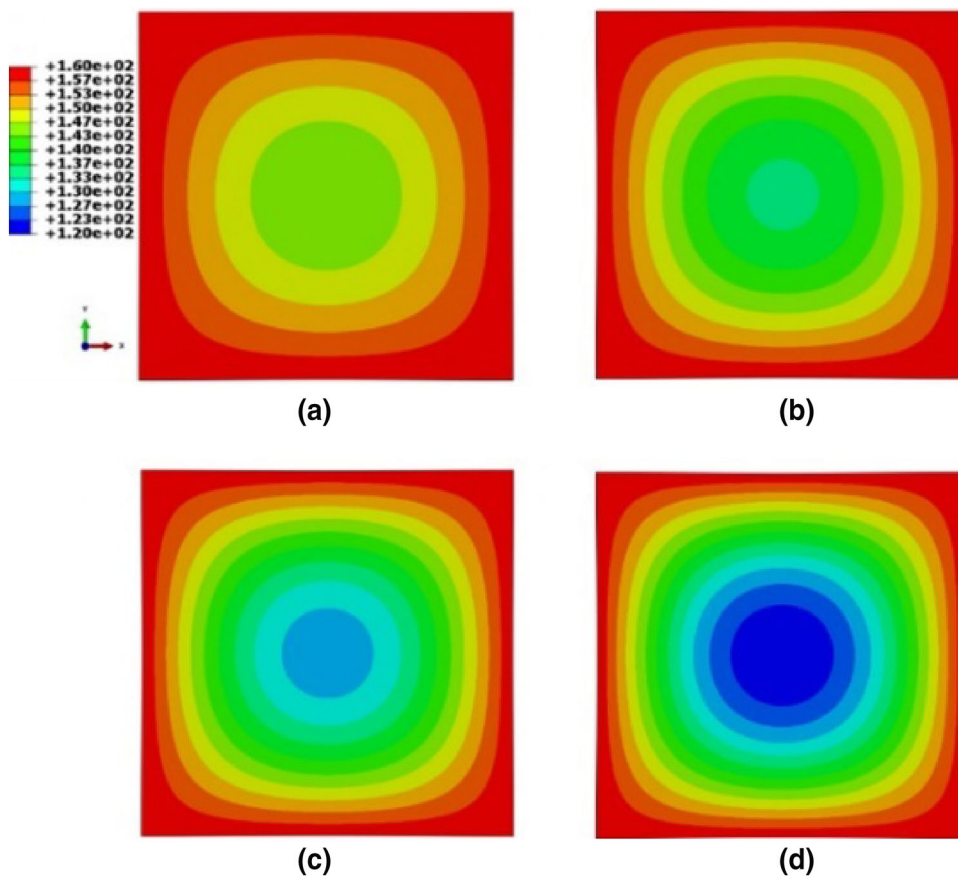


Fig. 3 (Color online) Neutron dose distribution (Unit: EDND). **a** Dose gradient = 10%, **b** dose gradient = 15%, **c** dose gradient = 20%, **d** dose gradient = 25%



creep modulus, E_{pc} , and Poisson’s ratio for primary creep, ν_{pc} .

The secondary creep strain, ϵ_{sc} , is defined as

$$\frac{d\epsilon_{sc}}{d\gamma} = \beta(1 - e^{-k_2\gamma})\mathbf{D}_{sc}\boldsymbol{\sigma}, \tag{4}$$

where k_2 is the secondary creep rate incubation dose constant, β is the saturated secondary creep rate parameter, and \mathbf{D}_{sc} is the secondary creep material matrix, which is a function of the secondary creep modulus, E_{sc} , and Poisson’s ratio for secondary creep, ν_{sc} .

In the new TMSR UMAT, the material properties E_e , E_{pc} , E_{sc} , ν_e , ν_{pc} , and ν_{sc} are all independent variables, that may have values different from their corresponding elastic properties.

2.3 Dimensional change strain

For a given irradiation fluence and temperature, the unrestrained dimensional change rate, subject to irradiation and weight loss, is given by

$$\frac{d\epsilon_{dc}}{d\gamma} = h(\vartheta, T, \omega), \tag{5}$$

where ϑ is the dose ratio, T is the temperature, and ω is weight loss.

2.4 Thermal strain

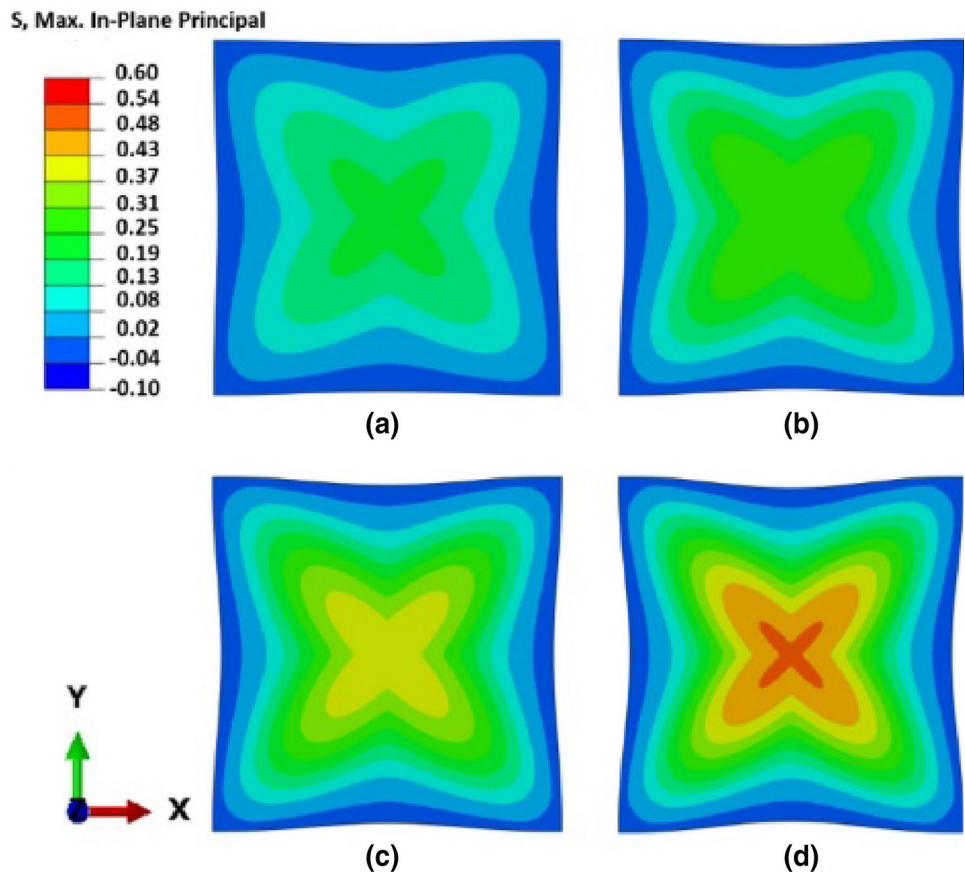
The thermal strain is defined as

$$\epsilon_{th} = \alpha_{(T_{ref}-T)}(T - T_{ref}), \tag{6}$$

where $\alpha_{(T_{ref}-T)}$ is the mean coefficient of thermal expansion between temperatures T_{ref} °C and T °C.

A comprehensive irradiated material property database is required for any graphite component stress analysis. The data required include irradiated elastic material properties, irradiation creep properties, irradiation-induced dimensional changes, and changes to the coefficient of thermal expansion. These properties are required as a function of fast neutron fluence, irradiation temperature, oxidation, and molten salt infiltration. Empirical irradiated material property data trends were derived from the analysis of data obtained by irradiating small samples in a Material Test Reactor (MTR). The units for the irradiation fluence and irradiation temperature are usually expressed in terms of equivalent DIDO nickel dose $\times 10^{20}$ n/cm² (EDND) [16] and temperature (°C), respectively. As the TMSR project is

Fig. 4 (Color online) Maximum principal stress of the graphite component without a permeation zone (MPa). The dose gradients for **a** through **d** are 10%, 15%, 20%, and 25%, respectively



in progress, no irradiation material properties for TMSR graphite could be obtained. For this study, the irradiated material property database was obtained from a gas-cooled reactor, PBMR. As the irradiation properties are commercially confidential, detailed information cannot be provided in this paper.

3 Finite element models of graphite component

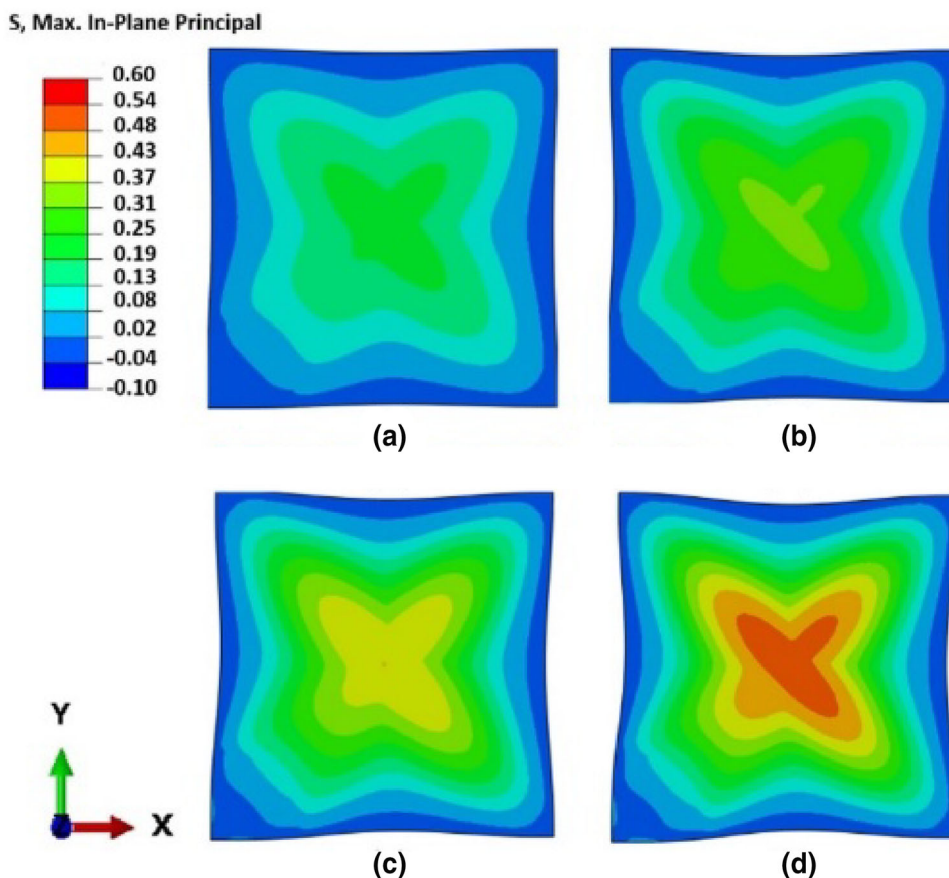
The graphite components used in the MSRE measured 2 inches square by about 6 feet long, were oriented vertically and rested on a grid of lattice support bars [11]. According to this, a primary graphite component was designed for the TMSR, with a cross section of 50 mm × 50 mm and a length of 1800 mm. Two assumptions were made to simplify the analyses of the nuclear graphite in the TMSR. First, supposing the graphite bars are completely immersed into the molten salt, and the fast neutron dose is a constant value within the surface which directly contacts the molten salt, the neutron dose varies with distance from the center to the boundaries of the graphite bar, but every cross section along its length has the same dose distribution. Second, a molten salt permeation zone, which includes numerous cracks or small open pores, allows molten salt to

enter the graphite bar. As previously discussed, the permeation zone has a higher temperature than the other zone and the fast neutron dose is as high as the area in immediate contact with the molten salt.

3.1 2D finite element models

A series of two-dimensional (2D) models were built based on the assumptions previously discussed. These 2D models were used to analyze the influence of the permeation zones and the irradiation dose gradient on the stress distribution of the graphite component. Three types of permeation zones were analyzed: a quarter circle in one corner, a half ellipse at the center of one edge, and a frame surrounding the boundaries. These are shown in Fig. 1. The size of the permeation zone was equated to the permeation area ratio (PAR) which was defined as the permeation zone area divided by the total model area. In these models, each type of permeation zone has four PAR values: 0.005, 0.02, 0.045, and 0.08. Moreover, the irradiation dose gradient was defined as the dose difference divided by the dose value at the boundaries of the model. The dose difference is the value at the boundaries minus the dose value at the center of the model; the boundary dose for all the models was the same. Each permeation area ratio model was

Fig. 5 (Color online) Maximum principal stress of the graphite component with a circular permeation area ratio of 4.5% (MPa). The dose gradients in subfigures a through d are 10%, 15%, 20%, and 25%, respectively



assigned four irradiation dose gradients (10%, 15%, 20% and 25%) to build different dose gradient models. As previously discussed, the dose value of the permeation zone is equal to the value at the model boundaries, which come in direct contact with the molten salt. The irradiation temperature in the rest zone was set to 650 °C, which is similar to the working temperature in the TMSR, while the temperature in the permeation zone was set at 750 °C due to molten salt retention in the permeated areas. The three models with PAR values of 0.005 are shown in Fig. 2. The finite elements used in this simulation were the eight nodes Generalization Plan Strain Element (CPEG8), which is typically used to model a section of a long structure that is free to expand axially, or is subjected to axial loading. The total numbers of elements for the three models were 2280 (quarter circle at one corner), 2704 (half ellipse at the center of one edge), and 2524 (frame surrounding the boundaries). The total numbers of nodes for the three models were 7037, 7775, and 8321, respectively.

A group of models were built without any permeation area present in the graphite component. The neutron dose was assumed as space-dependent. Figure 3 shows the dose distributions of different dose gradient models at the end of ten full power years. The dose gradients for the models (a) through (d) are 10%, 15%, 20%, 25%, respectively.

The tensile strength of graphite is much less than its compressive strength. According to the theory of maximum stress, the main cause of rupture in graphite should be the maximum tensile stress. In this study, the maximum tensile stress was equated to the maximum principal stress and used to analyze the internal stress of the graphite component. The maximum principal stress results were normalized by the peak maximum principal stress value from all the models analyzed in this paper.

The stress results are shown in Fig. 4, with the same dose gradients for (a) through (d) as in Fig. 3. It is clear that the maximum principal stress of the graphite component increases as the dose gradient increases. The peak maximum principal stress value exists at the center of the graphite component, meaning damage is initiated from this point when the stress reaches the rupture limit. The stress distributions within the graphite component were found to be symmetrical and the stress decreases from their central point to their boundaries. The outer surface was compressive.

Taking the permeation zones into consideration, a series of models with different permeation areas were built to explore the influence of various shapes and areas on the stress of the nuclear graphite component. Figures 5, 6 and 7 display the maximum principal stress distribution of the

Fig. 6 (Color online) Maximum principal stress of the graphite component with an elliptical crack area ratio of 4.5% (MPa). The dose gradients of the subfigures **a** through **d** are 10%, 15%, 20%, and 25%, respectively

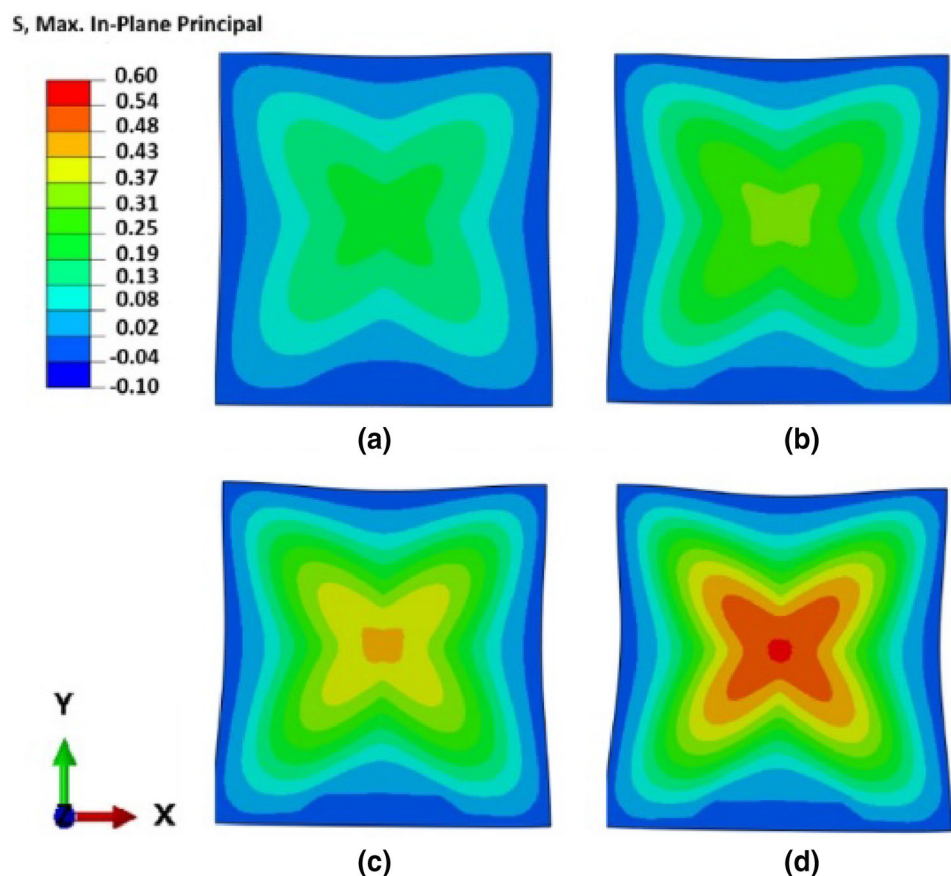


Fig. 7 (Color online) Maximum principal stress of the graphite component with a frame crack area ratio of 4.5% (MPa). The dose gradients of the subfigures **a** through **d** are 10%, 15%, 20%, and 25%, respectively

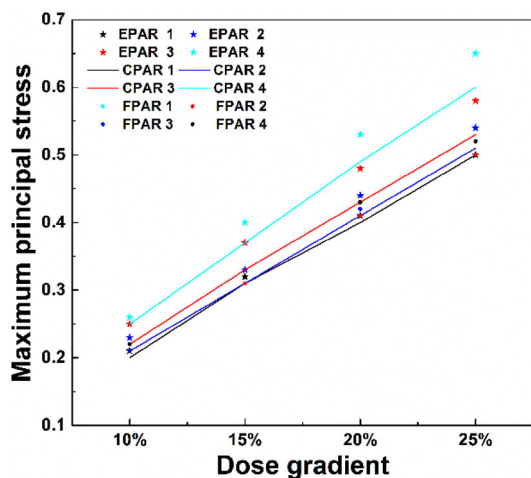
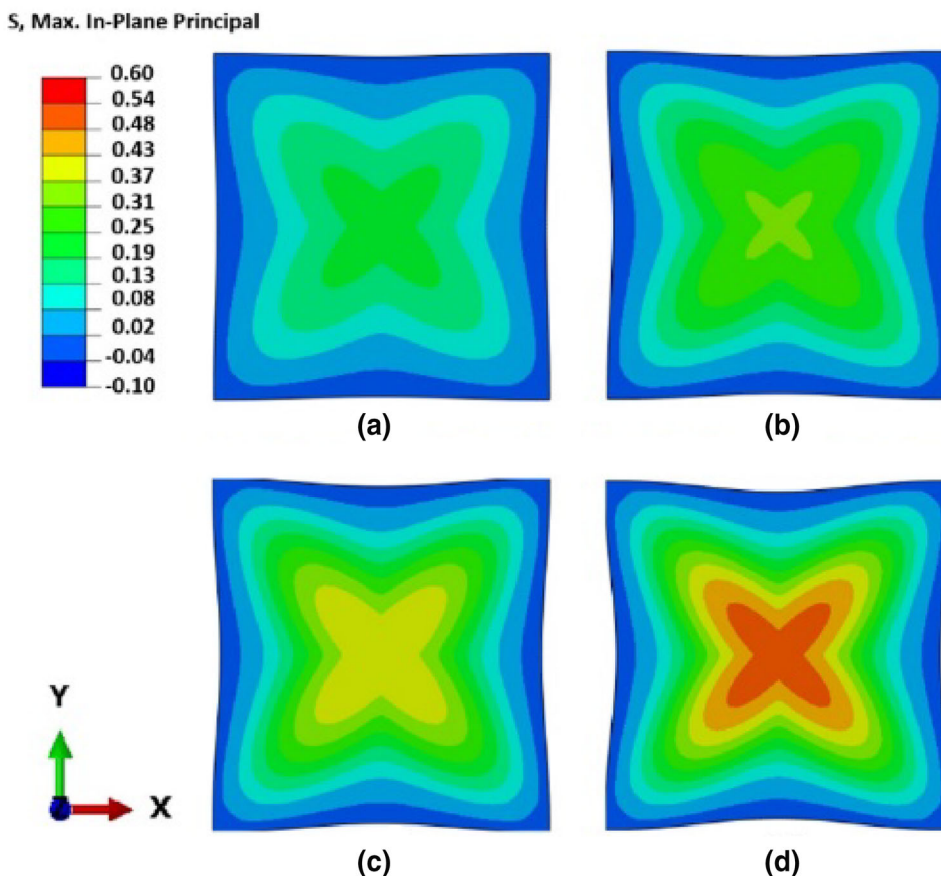


Fig. 8 (Color online) Peak value of the maximum principal stress for all permeation models (MPa). PAR = permeation area ratio, E for the half ellipse permeation zone, C for the quarter circle and F for the frame. The permeation area ratios of 0.005, 0.02, 0.045 and 0.08 are simplified to 1, 2, 3, 4, respectively

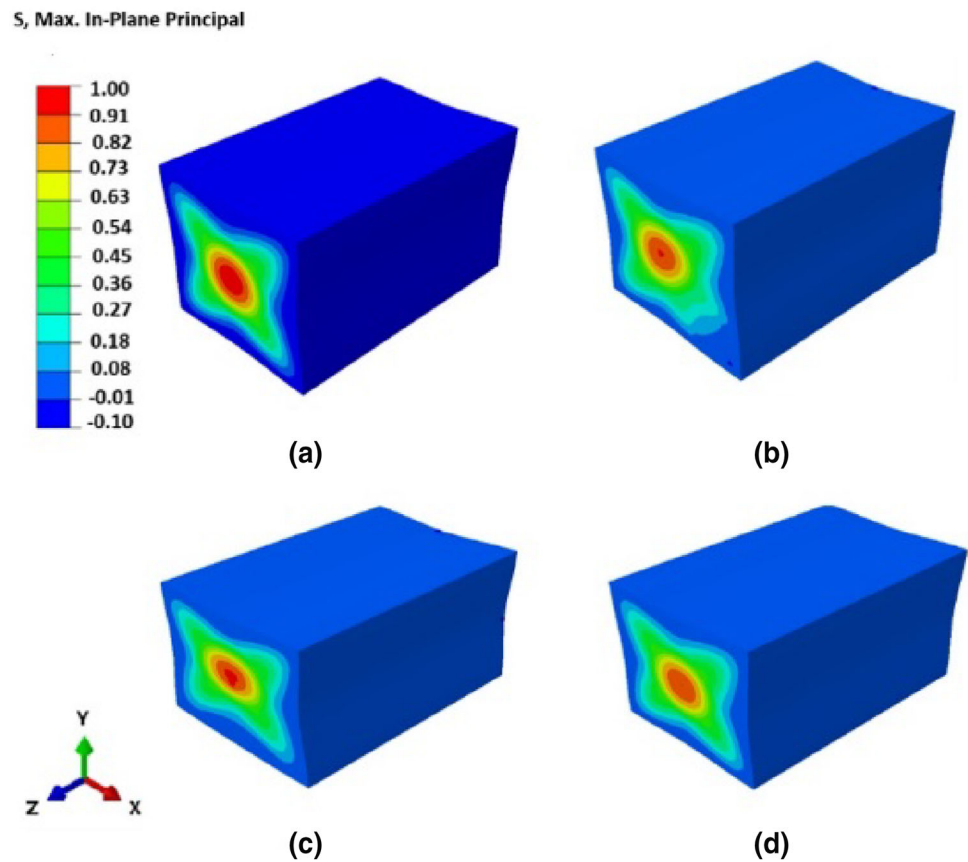
graphite component with a quarter circle, half ellipse, and a frame permeation zone, respectively. The permeation area ratios for these models are 0.045, and the dose gradients are as in Fig. 3. Some details agreed well with the results from the permeation zone-free models: For any given

permeation area, the maximum principal stress increases as the dose gradient increases, and the peak value of the maximum principal stress always occurs at the central point of the graphite component. However, the maximum principal stress was no longer symmetrical in the quarter circle and half ellipse permeation zone models. Moreover, the larger the permeation area was, the greater the damage was. While the stress distributions of the frame permeation zone models are similar to the preliminary permeation-free models, this could be because the frame permeation area is uniformly distributed around the graphite component. The peak values of the maximum principal stress for all permeation models are shown in Fig. 8. It can be seen that for any given dose gradient, the peak value of the maximum principal stress increases as the permeation area increases. For the cases estimated here, half ellipse permeation zones influence the stress distribution the most, and the influence from the frame permeation zones was the least significant. This could be because the half ellipse and quarter circle zones allow for the most intensive salt permeation.

3.2 3D finite element models

Four three-dimensional (3D) finite element models were built to verify the stress results from the 2D finite element

Fig. 9 (Color online) Maximum principal stress of a 3D graphite component with different permeation zones (MPa). **a** No permeation zone, **b** a quarter circle permeation zone in one corner, **c** a half elliptical permeation zone at the center of one edge, **d** a frame permeation zone around the boundaries



models. These models' cross sections measured $50\text{ mm} \times 50\text{ mm}$, and their length was 1800 mm . All the permeation area ratios of these models were 0.045 , and their dose gradients were 25% . These models include the three previously discussed permeation zones. The graphite brick is a deformable body, and so C3D20 elements were used to model its behavior. Rigid body motion was performed from the center of the body. The upper and lower surfaces were modeled as free boundaries. Figure 9 shows the stress results from these permeation models. The peak value of the maximum principal stress still occurs at the center of the graphite component in each permeation model. These different permeation zones produced different maximum principal stress modification amounts and shapes, affecting the symmetry to different degrees. The modification from the quarter circle was the largest and that from the half ellipse was found to be the second most influential, while the stress distribution from the frame permeation zone is similar to the models which were free of permeation zones.

4 Conclusion

In this paper, a User Material (UMAT) subroutine, containing irradiation-dependent constitutive relationships for graphite dimensional changes and the material properties of graphite, was utilized to perform initial stress analysis of a graphite component. The irradiated material property database was obtained from a gas-cooled reactor, due to the lack of an irradiated properties database for the TMSR-specific graphite. The stress analysis shows that for a regular graphite component with a square cross section, the peak maximum principal stress value occurs at the center of the cross section, which suggests that the damage will begin from this point if the stress reaches the rupture limit. Furthermore, the dose gradient, the shape, and the area of the permeation zone all significantly influence the stress distribution. First, for each permeation zone modeled, the larger the dose gradient was, the larger the maximum stress was. Second, for each dose gradient of any shape permeation zone, the greater the permeation area was, the higher the peak maximum principal stress value was at the center of the graphite component. Lastly, the symmetry of the maximum principal stress distributions were significantly modified by the quarter circle and the

half ellipse permeation zones. For the same permeation zone shape, the larger the permeation area was, the more significant the damage was. For the same permeation area, the more concentrated the permeation zone was, the greater the damage was.

References

1. E.S. Bettis, R.W. Schroeder, G.A. Cristy et al., The aircraft reactor experiment-design and construction. *Nucl. Sci. Tech.* **2**(6), 804–825 (1957). <https://doi.org/10.13182/NSE57-A35495>
2. P.N. Haubenreich, R.J. Engel, Experience with the molten-salt reactor experiment. *Nucl. Appl. Technol.* **8**(2), 118–136 (1970). <https://doi.org/10.13182/NT8-2-118>
3. Y. Shimazu, Nuclear safety analysis of a molten-salt breeder reactor. *J. Nucl. Sci. Technol.* **15**(7), 514–522 (1978). <https://doi.org/10.1080/18811248.1978.9735543>
4. T. Abram, S. Ion, Generation-IV nuclear power: a review of the state of the science. *Energy Policy* **36**(12), 4323–4330 (2008). <https://doi.org/10.1016/j.enpol.2008.09.059>
5. L. Samalova, O. Chvala, G.I. Maldonado, Comparative economic analysis of the Integral Molten Salt Reactor and an advanced PWR using the G4-ECONS methodology. *Ann. Nucl. Energy* **99**, 258–265 (2016). <https://doi.org/10.1016/j.anucene.2016.09.001>
6. T. Schönfeldt, E.B. Klinkby, K.H. Klenø et al., Conceptual design of a thorium supplied thermal molten salt wasteburner. in 17th Meeting on Reactor Physics in the Nordic Countries, Göteborg, Editor (Sweden, 2015)
7. S.R. Greene, J.C. Gehin, D.E. Holcomb et al., *Pre-Conceptual Design of a Fluoride-Salt-Cooled Small Modular Advanced High Temperature Reactor (SmAHTR)* (Oak Ridge National Laboratory (ORNL), Oak Ridge, 2011)
8. Z.T. He, L.N. Gao, W. Qi et al., Molten FLiNaK salt infiltration into degassed nuclear graphite under inert gas pressure. *Carbon* **84**, 511–518 (2015). <https://doi.org/10.1016/J.CARBON.2014.12.044>
9. Y. Zhong, X. Yang, D. Ding et al., Numerical study of the dynamic characteristics of a single-layer graphite core in a thorium molten salt reactor. *Nucl. Sci. Tech.* **29**, 141 (2018). <https://doi.org/10.1007/s41365-018-0488-8>
10. K. Furukawa, L.B. Erbay, A. Aykol, A study on a symbiotic thorium breeding fuel-cycle: THORIMS-NES through FUJI. *Energy Convers. Manag.* **63**(6), 51–54 (2012). <https://doi.org/10.1016/j.enconman.2012.01.030>
11. G.W. Scherer, Stress from crystallization of salt. *Cem. Concr. Compos.* **34**(9), 1613–1624 (2004). <https://doi.org/10.1016/j.cemconres.2003.12.034>
12. R.B. Briggs, W.H. Cook, A. Taboada, Modifications to Specifications for MSRE Graphite. 1963: United States. <https://doi.org/10.2172/1334752>
13. D.K.L. Tsang, B.J. Marsden, Constitutive material model for the prediction of stresses in irradiated anisotropic graphite components. *J. Nucl. Mater.* **381**(1–2), 129–136 (2008). <https://doi.org/10.1016/j.jnucmat.2008.07.025>
14. D.K.L. Tsang, B.J. Marsden, The development of a stress analysis code for nuclear graphite components in gas-cooled reactors. *J. Nucl. Mater.* **350**(3), 208–220 (2006). <https://doi.org/10.1016/j.jnucmat.2006.01.015>
15. D.K.L. Tsang, B.J. Marsden, Effects of dimensional change strain in nuclear graphite component stress analysis. *Nucl. Eng. Des.* **237**(9), 897–904 (2007). <https://doi.org/10.1016/j.nucengdes.2006.01.015>
16. B.J. Marsden, M. Haverty, W. Bodet et al., Dimensional change, irradiation creep and thermal/mechanical property changes in nuclear graphite. *Int. Mater. Rev.* **61**(3), 155–182 (2016). <https://doi.org/10.1080/09506608.2015.1136460>